Advances in Science and Technology Research Journal

Advances in Science and Technology Research Journal 2022, 16(4), 232–242
https://doi.org/10.12913/22998624/152529
ISSN 2299-8624, License CC-BY 4.0

Received: 2022.06.06
Accepted: 2022.08.22
Published: 2022.09.01

Microstructure and Properties of Dissimilar Joints of AISI 430 Steel with Inconel 625 Obtained by Electron Beam Welding

Małgorzata Dziekońska[1], Ewa Jonda[1], Marek Sroka[1*], Marek Węglowski[2], Tymoteusz Jung[3]

[1] Department of Engineering Materials and Biomaterials, Faculty of Mechanical Engineering, Silesian University of Technology, Konarskiego 18a, 44-100 Gliwice, Poland

[2] Łukasiewicz Research Network – Welding Institute Gliwice, B. Czesława 16-18, 44-100 Gliwice, Poland

[3] Łukasiewicz Research Network – Institute for Ferrous Metallurgy, K. Miarki 12-14, 44-100 Gliwice, Poland

* Corresponding author's e-mail: marek.sroka@polsl.pl

ABSTRACT

Electron beam welding (EBM) is a high-energy density fusion process where joint is bombarded to be welded with strongly focused beam of electrons. This method is often used for advanced materials and complex, critical parts, like turbine rotors, but it can also be used for many simpler processes involving large production runs. It is very suitable for butt welding materials of different thicknesses. The aim of this work was to study the microstructure, hardness, and electrochemical corrosion behavior between the dissimilar welds were investigated. Electron Beam Welding of dissimilar steel alloys Inconel 625 and AISI 430 was studied. In welding process there was used only welded materials without filling material. Results showed the microstructure of the weld solidified in dendritic morphology. The microstructure of fusion zone showed that dendrites grew in different directions for each grain. The dendrites and columnar grains are mainly exposed to the fusion boundary with some equiaxed grains. The hardness of the overall joint was non-uniform. The highest hardness of the HAZ/Inconel 625 (the heat-affected zone) was 258 HV, and the lowest weld zone hardness was 178 HV. The decrease in weld hardness may be due to the linear welding energy, which led to grain growth and excessive cooling. HAZ/AISI 430 steel has the lowest current density and the highest corrosion potential. Steel has a more negative corrosion potential and a lower corrosion current density than joints, likely due to higher levels of chromium. In this study, a metallographic investigation of the joints revealed no defects such as microcracks or pores. The melting temperatures of the two materials were quite different, but with the help of gravity, stainless steel acts as a permanent joint, like a rivet.

Keywords: dissimilar joint, Inconel 625, AISI 430 stainless steel, electron beam welding, microstructure, properties

INTRODUCTION

Due to its high strengths and good corrosion resistance, stainless steel is used extensively in industry. AISI 430 steel is very popular and characterized by high corrosion resistance, easy treatment, and relatively low cost. This allows use when stainless steel is required and the operating temperature does not exceed 750 °C – engineering industries, construction, architecture, and household appliance production [1-5].

Inconel belongs to a group of nickel-chromium superalloys (so-called Super Alloys) containing up to 20% Cr, 20% Mo, and up to 10% Fe, as well as small additions of Si, Mn, Ti, Nb, V, or W [6, 7]. These heat-resistant nickel alloys are mainly used for rotor blades and nozzles in gas turbines, rocket and jet engines, and elements of chemical apparatus, operating at high temperatures, and for gas corrosion. The main advantages of Inconel alloys are high oxidation and corrosion resistance, and good adaptation for work in extreme conditions [8, 9]. When heated, Inconel creates a thick, stable layer that protects the surface against attacks (it passivates when heated).

Superalloy Inconel 625, due to its high corrosion resistance and good strength properties at high temperatures, is used in the aviation industry [10].

Forming this material is conducted using plastic treatment methods; however, it shows significant deformation strengthening. According to standards, thin sheets should have minimum yield strength of 415 MPa, a tensile strength of 830 MPa, and an elongation to break of at least 30% [11]. Manufacturers usually supply materials with yield points of ~500 MPa, which does not allow them to be cold-formed to obtain elements with complicated shapes (too little deformation). However, an appropriately performed softening treatment produces a yield point below 400 MPa and an elongation to break of 70% [12], even by increasing the processing temperature – up to 110%. However, the temperature cannot be raised arbitrarily because supersaturation aging occurs above 550 °C, which rapidly reduces the plasticity of the alloy [13].

The combination of stainless steel and Inconel alloy yields materials that work in conditions necessary for gas turbines, reactors, or rocket engines. These materials have much better strengths, toughness, and good corrosion resistance at elevated temperatures. This afforded materials with better structures, which were more economically profitable [8, 9].

Welding is one method to join these materials [14]. However, very serious metallurgical and technological problems may arise during welding, which primarily stems from differences in the physicochemical properties of materials, such as the melting point, thermal conductivity or expansion coefficients, or the weld material structure. This may be locally altered due to the formation of weld metal from the binder and parent material (especially in the weld transition zone), which leads to brittle cracks in the weld or increases the tendency to crack at elevated temperatures. Moreover, the transition zone of the weld is physically and chemically "discontinuous", which may reduce the functional properties of the joint – showing a greater tendency for selective corrosion [15, 16]. Metallurgical issues related to the melting and solidification, such as segregation of elements, solidification cracking, and liquation cracking may occur [17-19]. Besides the chemical composition of the parent material, welding process parameters play a major role in microstructural features. This factor also effectively influences weldability, corrosion resistance, and mechanical properties. The welds of electron-beam welded joints are characterized by high purity because the vacuum during welding ensures the continuous discharge of gases emitted from the weld pool and the potential for a narrow weld and a narrow HAZ.

During electron beam welding (EBW), a material is heated and joining points are fused by a focused stream of electrons, whose source is an electron gun with a heated cathode, and electrons are accelerated by tens and sometimes even hundreds of kV. Electron welding most often occurs under vacuum, at pressures of ~10^{-4} hPa, and the weld is formed by fusing edges of parts to be joined [20, 21]. The vacuum surrounding the workpiece prevents the formation of gas pores or porosity in the weld, as gas molecules are immediately removed, and prevents the weld from oxidizing. The use of this method, compared with conventional methods, enables deep remelting, a small joint width, a small heat-affected zone, slight deformation, and strength that approximates the parent material (Fig. 1) [3, 22].

In many cases, EBW remains indispensable due to its greater penetration depth and metallurgical cleanliness of the weld, as well as high welding speeds. EBW finds use in surfacing, remelting, alloying, rapid prototyping, making holes (perforating), producing gradient materials, and many other applications. In EBW, materials can be combined in width range so dissimilar joints play an important role. Literature reports contain information regarding possible unfavorable combinations. In this method, heat comes from the impact of the high-energy electron beam, and electrons emitted by the gun accelerate to speeds ~30–70% of light speed. Their high kinetic energies during contact with the workpiece release the heat necessary to achieve a weld. EBW of pure nickel or

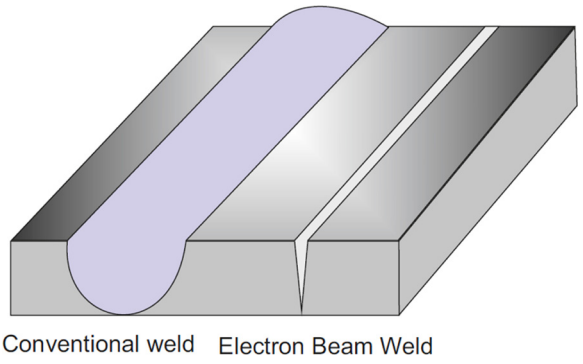

Figure 1. Comparison of conventional and electron beam welds

nickel-copper alloys and many nickel-iron alloys are done without major problems [23, 24]. The welding advantages of this method include high power density, potential to control the weld penetration depth, no harmful external factors influencing the melted and heated materials, and very low deformation of the welded elements [15, 25].

So far, literature reports provide only Inconel test results – stainless steel made in other ways, e.g., GTAW or laser welding [26-28]. This study sought to determine the structure, mechanical properties, and corrosion resistance of a dissimilar joint of AISI 430 steel with Inconel 625 welded using EBW, which has not yet been widely tested.

MATERIALS AND METHODS

The materials used were specimens of dissimilar welded joints made from ferritic stainless steel AISI 430 and Inconel 625 obtained by the EBW method. In Table 1 chemical composition of used materials is shown. Samples have about 25×50 mm.

Electron beam welding (EBW) was performed on the universal EB welding system type XW150:30/756 (Cambridge Vacuum Engineering) and conducted using the parameters presented in Table 2.

Microstructure study

For microstructural analyses, a cross-section of the dissimilar joint was prepared along the welding direction. Two stage etching was used: first chemical one in Marble reagent, second electrochemical etching in Cr_3O_2 solution - 2A current, 10-15 seconds. The microstructure of the dissimilar joint was examined using a scanning electron microscope (Inspect F, FEI, Japan). The detection of secondary electrons (SE), with acceleration voltages between 20V –300 kV and a maximum magnification of 2000000 times obtained sample images. Microstructure investigations were conducted on metallographic microsections made on the cross-section of tested samples of components in the weld area. They were prepared by mechanical grinding, polishing, and etching. Observations were made with magnifications up to 8000x.

A laser scanning confocal microscope (LSM5 Excite Zeiss Company, Jenna, Germany) was used to observe the topography and roughness of the surface weld. Samples were prepared in the as-welded weld zone.

Mechanical properties

Vickers microhardness was made at low load force 9.81N - HV1 to investigate the hardness of various zones in the welded joint. The hardness was measured on samples taken for metallographic investigations (metallographic specimens). They contained the weld joint centerpiece and were cut perpendicular to the weld. The line through which the hardness tests were performed ran through the welded joint center thickness section. Hardness was measured in the following areas: Inconel substrate material, HAZ/Inconel, weld, HAZ/steel, and steel.

Corrosion tests

Corrosion experiments were conducted in a conventional three-electrode cell with platinum and saturated calomel SCE electrodes as the counter and reference electrodes, respectively. Electrochemical corrosion resistance tests were carried out using a Potentiostat / Galvanostat ATLAS 0531 EU (Atlas-Sollich Company), as per standard [29], and were implemented in two stages:

Table 2. Parameters of electron beam welding

Parameter	Value
Acceleration voltage (kV)	140
Current beam (mA)	4
Focal distance (mA)	700
Filament (A)	22
Welding speed (mm/min)	500

Table 1. Chemical composition of stainless steel AISI 430 and Inconel 625

Material	Chemical Composition, %							
AISI 430	C	Mn	Si	P	Cr	Ni		
	<0.08	<1.0	<1.0	<0.04	<0.015	16.0-18.0		
Inconel 625	Fe	Co	Si	P and S	Cr	Ni	Mo	Nb
	<5.0	<1.0	<0.5	<0.15	20.0-23.0	>58.0	8.0-10.0	3.15-4.15

Determination of the open circuit potential in no-current conditions

Potentiodynamic polarization from the starting potential is less than 100 mV. The rate of potential increase was 1 mV/s; conditions to stop the polarization included the following thresholds: 1V by potential or 1mA by the current. Corrosion tests were performed in aqueous 0.1 M NaCl. These results were determined using the Tafel extrapolation method. The device parameters are presented in Table 3.

All solutions were prepared using an analytical reagent from Merck and doubly distilled water. Samples were abraded with wet SiC abrasive papers at grits of 220, 400, 600, 800, 1000, 1200, and 2000, by a mechanical instrument model Struers LaboPol-1, degreased using acetone, rinsed with distilled water, and dried with dry air. Afterward, all samples were polished using 1 μm diamond paste, polished again with 0.05 μm alumina, rinsed with water, washed with ethanol, and sonicated before each electrochemical experiment.

Table 3. Technical data of potentiostat ATLAS 0531 EU

Number of electrodes connected	Max 5
Linear operating range of the electrode, V	10
Maximum current of the tested electrode, A	2
Potential accuracy %	~2
Input impedance, TOhm	>1
Software	NOVA 1.11

RESULTS AND DISCUSSION

Figure 2 shows the welded joint and scanning electron microscope microstructures of the parent materials. Visual analysis and macrostructure examination revealed that dissimilar welds obtained using EBW were properly fused, and no damages were observed. The weld bead profile was good and free from cracks. Microstructures were made on the "top" side of weld.

Welded samples with full penetration were chosen and cut from the weld seam cross-section to investigate the microstructure. Figure 3 gives a cross-section macro-photograph showing the electron beam welds of Inconel 625 and AISI 430 – it contains the center of the welded joint and was cut perpendicular to the seam.

Figure 4 shows the microstructure investigation results from SEM. This figure shows several welded joint parts: parent material, HAZ, and weld. EBM shows a narrow HAZ due to very low heat inputs and extremely localized heating.

The microstructure of the welds showed they solidified with dendritic morphology. Fusion zone microstructures showed that dendrite direction growth differed in each grain. The fusion boundary revealed mainly dendrites and columnar grains with some equiaxed grains, and agrees with results from Emadi [30]. A competitive growth between the grains and solidification boundaries was revealed, these boundaries are the interface between "packets" with aligned dendrites (Fig. 5).

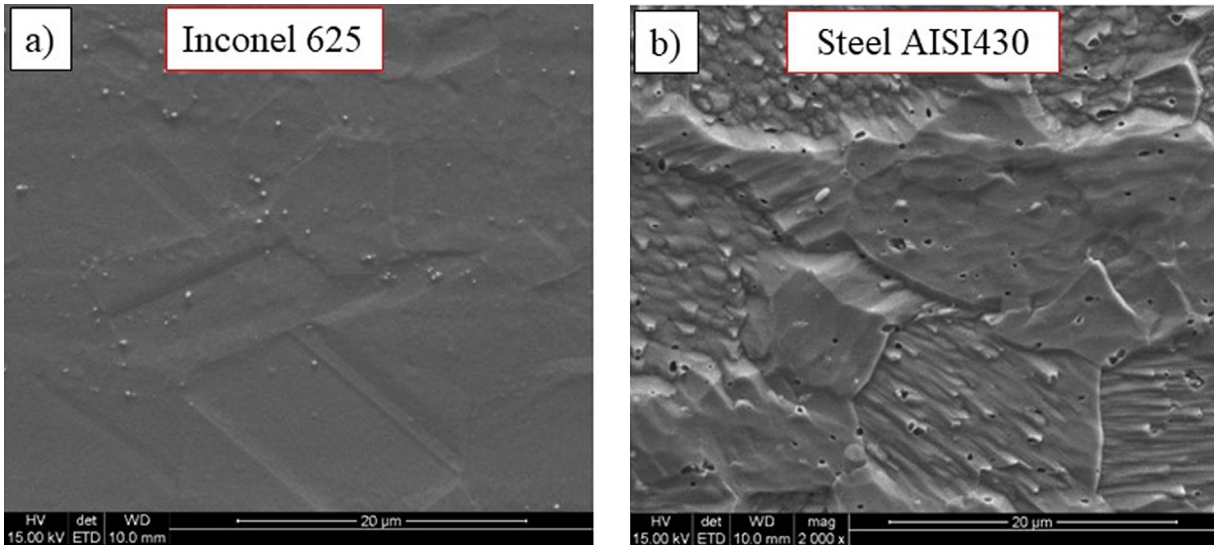

Figure 2. Microstructures of base metals a) Inconel 625 and b) AISI 430

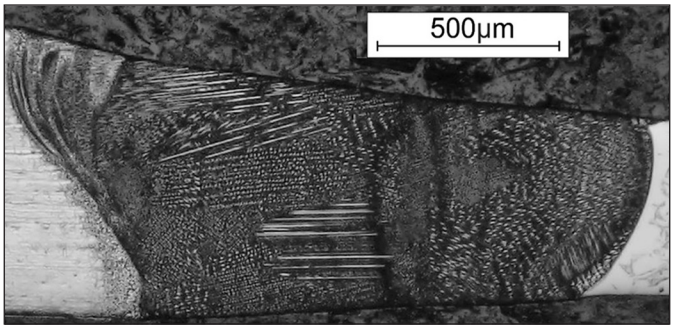

Figure 3. Cross-section macro-photograph showing electron beam welds of Inconel 625 and AISI 430

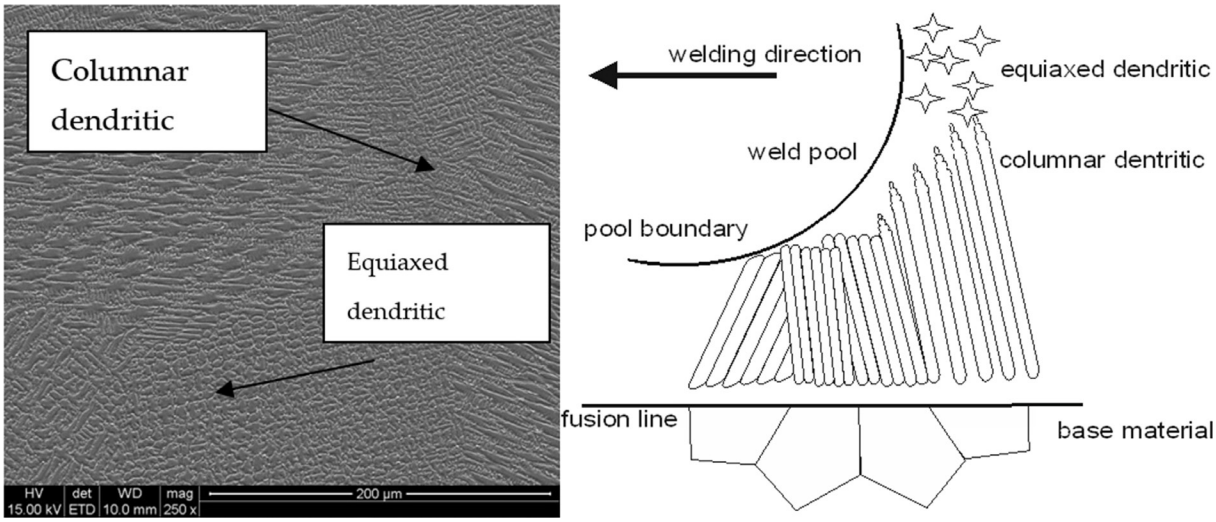

Figure 4. Microstructure of the parent material (a, b), HAZ (d, e), and the weld (c)

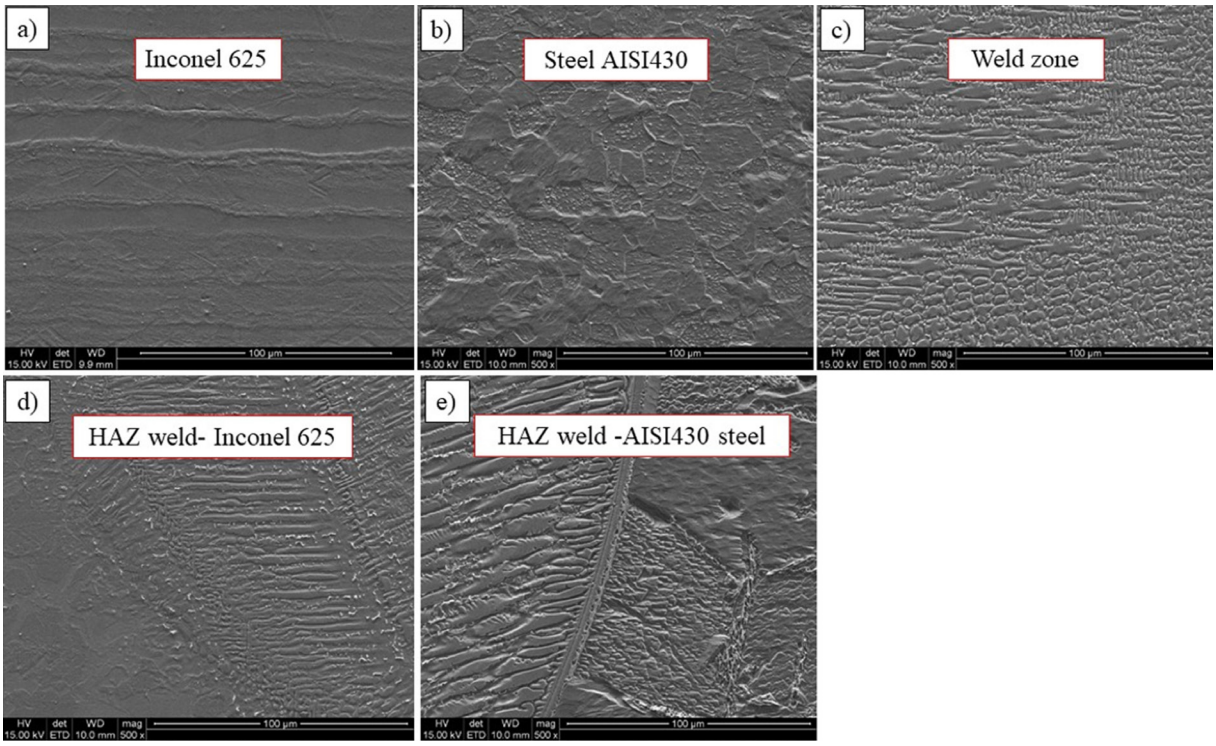

Figure 5. a) Microstructure from the weld of Inconel 625 and AISI 430, b) variation in solidification mode across the fusion zone [30]

Major alloying elements in Inconel 625 (Nb and Mo) tend to segregate during rapid weld solidification, which leads to high undercooling and the formation of a very fine structure. The undercooling difference leads to the formation of a columnar dendritic structure and a second phase between these areas (Fig. 6). The weld microstructure near HAZs has a columnar dendritic structure. Heat input influences the weld microstructure. At constant welding speed, the temperature gradient decreased while the increased heat input decreased undercooling at the solid/liquid front, so an equiaxed structure should form (Fig. 4). This structure forms along the centerline which creates a columnar dendritic structure near the fusion line [30]. No solidification or liquation cracking was observed. Weld metal microstructures near HAZs had columnar dendritic structures, which created a composition gradient in those areas.

A rapid weld metal cooling rate was responsible for the very fine dendritic structure formation in the weld fusion zone. The solidification rate significantly influences the segregation of alloying elements and is restricted at high solidification rates. This causes significant differences between the microstructure of a solidified casting alloy and a solidified weld. Nickel, chromium, and iron distribution coefficients were all > 1, which led to segregation of alloying elements into the dendrite core, while niobium in nickel-based alloys was < 1 and segregated into interdendritic spaces [31].

Laser scanning confocal microscopy characterized the topography and roughness of the welds. Samples were prepared from the as-welded weld zone. Three places were chosen to observe the weld quality obtained by EBW – two ends of the weld and the center. Figure 7 shows the laser confocal microscopy results including the weld seam thickness distribution. Table 4 lists the surface roughness values Ra, which represents the irregularity of the surface profile for each sample.

The lower rectangle shown in Figure 7 highlights the profile roughness parameters. The upper rectangle indicates areal roughness parameters. Profile roughness values determined during Ra measurement and areal roughness, RSa are shown in Table 4.

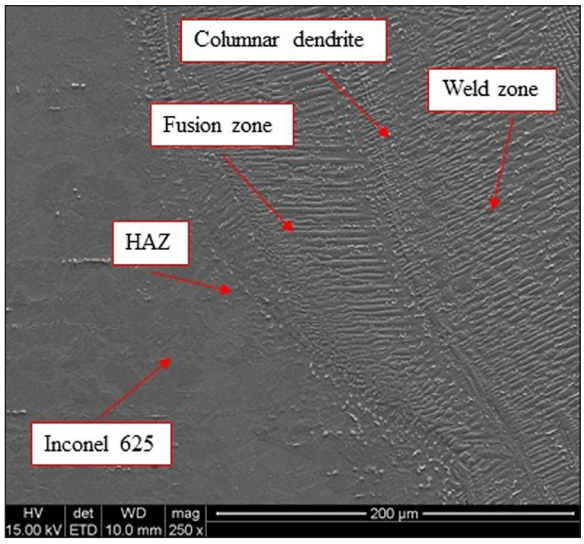

Figure 6. Microstructure of weld and Inconel 625

According to this table, the surface roughness values recorded at test points located at the welded joint "ends" are larger than those obtained from the weld center. The roughness profile in the center ("point 2'") was more homogenous than the "end" ones.

Hardness

Hardness was measured on samples taken for metallographic investigations (metallographic specimens). They contained the weld joint centerpiece and were cut perpendicular to the weld. The line along which hardness tests were performed ran through the center thickness section of the welded joint. Hardness was measured in the following areas: Inconel substrate material, HAZ/Inconel, weld, HAZ/steel, and steel. Directions of hardness analysis and measuring spots were set in characteristic zones for metallographic sample cross-sections, so they run through the parent metal, the heat-affected zone, and the weld metal. Figure 8 shows the hardness distributions for all of those directions.

A hardness profile is a good tool to evaluate the hardness of the entire joint [32, 33]. Five measurements were made for each zone, two of which were rejected (min/max) while maintaining the appropriate distance interval of four times

Table 4. Electron bean welding parameters

Parameter	A	B	C
Profile roughness, Ra, µm	6.476	5.630	7.751
Areal roughness, RSa	5.803	4.408	7.737

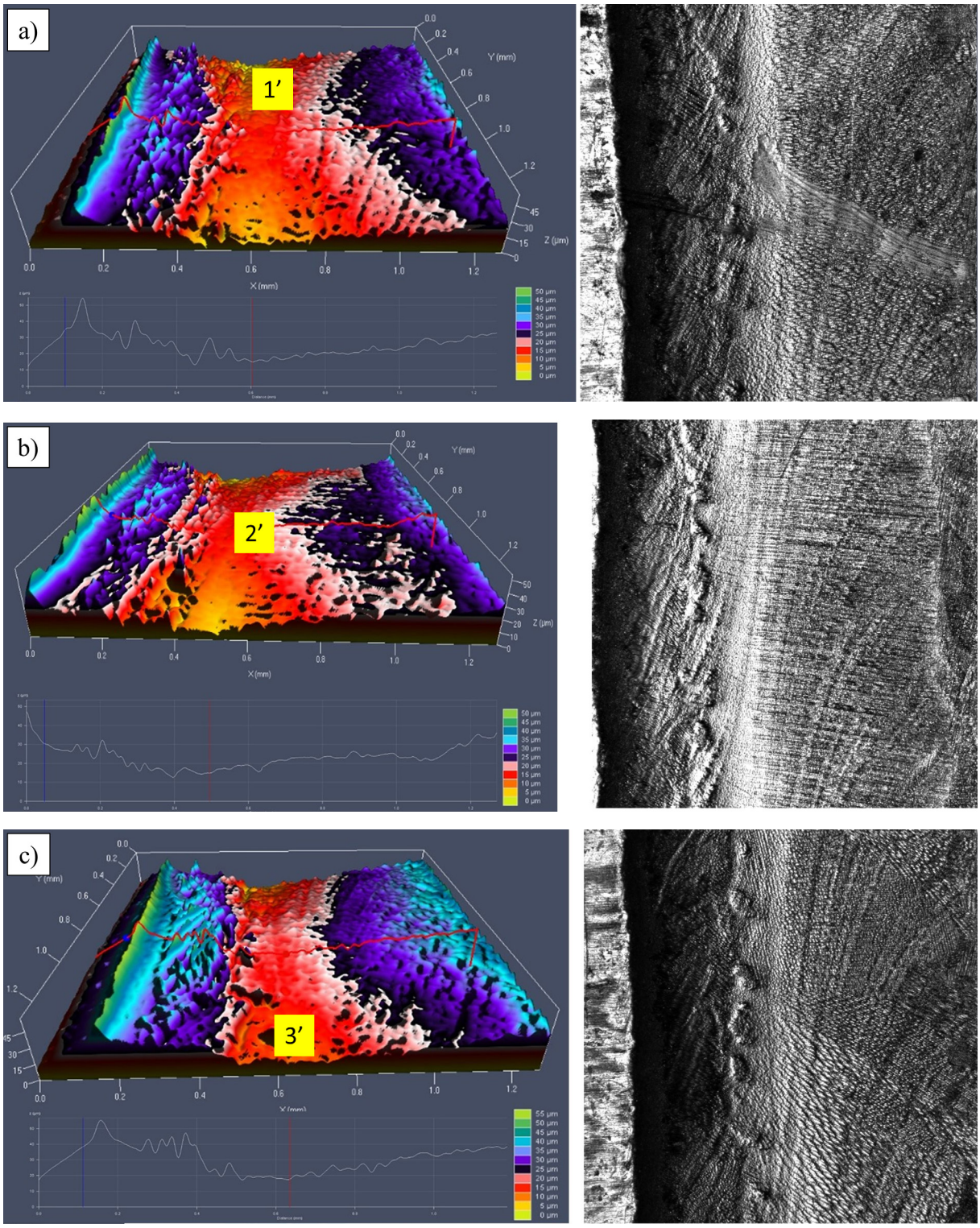

Figure 7. Laser confocal microscopy of specimens including the weld seam thickness distribution in different places a) point 1', b) point 2', and c) point 3'

the indenter size to avoid the effects of localized strain hardening in the vicinity of the indentation. Finally, the averages of the three measurements were reported. Hardness studies were carried out across the cross-section of a dissimilar weld from Inconel 625 and AISI 340 steels. During welding, the hardness of the weld itself depends on the welding method and its conditions. As a rule, the weld hardness itself is the result of materials that have been welded together, but the lowest hardness occurs in the weld itself. This may be due to tempering effects and the presence of nickel.

Figure 8. Distribution of hardness results in HV1 measured on transverse microsections of the welded joint

The hardness profile shows that HAZ had the maximum hardness when compared to the weld. The higher hardness occurred due to the brittle phases of Cr and Ni precipitation in HAZ. The average hardness of the entire weld was ~230 HV1. The lower weld hardness may result from grain growth stemming from the influence of linear welding energy and, at the same time, too high a cooling rate. There was a hardness increase in the direction from the axis of the weld to the HAZ. The temperature required for recrystallization over a very short period (seconds) was 850 °C and occurred up to 2 mm from the weld. Recrystallization occurs between the grain growth region and 2 mm from the weld near the top. The recrystallization resulted in hardness of approximately 188 HV1. The hardness over 2 mm from the weld increased - in HAZ/Inconel, the hardness was 257 HV1, while HAZ/steel was approximately 246 HV1. There are still elevated temperatures that temper the material and tempering may occur in these zones. Tempering decreases hardness and has a higher effect closer to the weld. Tempering does not affect material > 5 mm from the weld.

Nickel-based superalloys have higher hardness than metals with fully ferritic structures. This may be related to the formation of different phases in this area. Hardness reduction in the weld itself may result from diffusion of solvent elements i.e., niobium and molybdenum from the solid lattice solution and microsegregation [25]. Hardness in HAZ in the vicinity of Inconel 625 exceeded that of AISI 430. Formation of more chromium carbide and a stronger solid solution due to a higher chromium concentration in the Inconel 625 may explain that observation. The lower hardness in the weld also stemmed from grain growth in this area. The size of the imprint influences the material hardness. With a small one, there is a possibility of hitting the "holes" created due to corrosion. The application of a low load can reduce the hardness within the joint [34].

Corrosion test

Potentiodynamic polarization plots for dissimilar joints in 0.01 M NaCl solution are shown in Figure 9. All polarization plots followed Tafel-style behavior. During potential anodic scanning, no active current peak was observed, and may be due to sample surface passivation by oxide films [35]. In Table 5, the corrosion potential, corrosion current density (Icorr), and resistance polarization are shown.

As seen in Table 5, the highest corrosion current value was characteristic for the weld, while the lowest value is in HAZ/steel. The highest polarization resistance was observed in HAZ/Inconel, while the lowest was in the weld. The highest corrosion potential was observed for steel, while the lowest was for HAZ/steel. Accounting for the above dependencies, the welded joint between the Inconel 625 alloy and AISI 430 steel was characterized by a reduced corrosion resistance compared to native materials. The corrosion potential of steel was more negative as compared to the welded

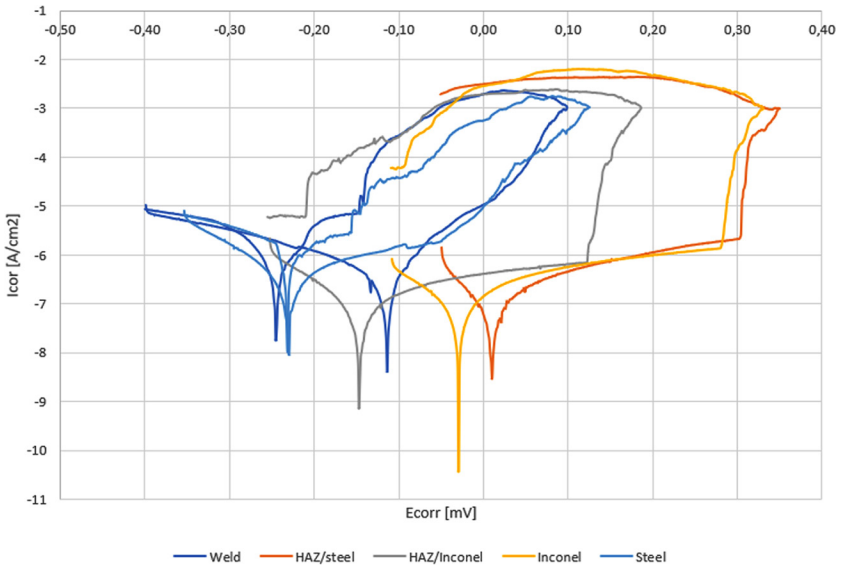

Figure 9. Potentiodynamic polarization curves for specimens in 0.1 M NaCl

Table 5. Corrosion results listing potential (Ecorr), protection (or repassivation) potential (Rp), passive current density (Ba), and corrosion rate (Bc)

Parameter	Icorr μA/cm^2	Ecorr 10-3V	Rp Ω·cm^2	Ba	Bc
Steel	339.70	-232.41	84.52	195.80	99.85
Weld zone	486.62	-117.44	53.83	82.76	222.56
HAZ/steel	59.80	9.51	230.99	71.80	57.11
HAZ/Inconel	79.49	-147.97	314.88	158.55	90.58
Inconel	79.35	-30.42	274.37	112.16	90.68

joint and showed a lower corrosion current density likely due to higher levels of chromium. Corrosion resistance tends to improve with added Cr, Cr and Mo improve resistance to local corrosion.

CONCLUSIONS

In EBW, stainless ferritic steel and superalloy Inconel welds are characterized by high purity, the potential for narrow welds, and a narrow HAZ. Visual analysis and macrostructure examination revealed proper fusion, no damages were observed, and the weld bead profile was good and free from cracks. Surface roughness values recorded at test points located in welded joint "ends" were larger than those obtained at the "center" of the weld and the roughness profile in the "center" was more homogenous than for "end" profiles.

The average hardness of the entire weld was approximately 230 HV1 and HAZs showed maximum hardness as compared to the weld seam, which may have resulted from grain growth due to the linear welding energy influence and, at the same time, too high of a cooling rate. Moreover, these results confirmed the high quality of the joint and showed that it meets strength and quality requirements.

HAZ/AISI 430 steel has the highest corrosion potential and shows lowest current density. Due to a higher amount of chromium steel shows a lower corrosion current density than joints. Even though EBW is an ideal fusion welding process, fusion zone changes (like defects) can sometimes occur that affect the shape and structure of the weld.

REFERENCES

1. Baddoo N.R. Stainless steel in construction: A review of research, applications, challenges and opportunities. Journal of Constructional Steel Research 2008; 64(11): 1199-1206.
2. Eskandari F., Atapour M., Golozar M.A., Sadeghi B., Cavaliere P. Corrosion behavior of friction stir processed AISI 430 ferritic stainless steel. Materials Research Express 2019; 6: 086532.

3. Li Y-F., Hong S-T., Choi H., Han H.N. Solid-state dissimilar joining of stainless steel 316L and Inconel 718 alloys by electrically assisted pressure joining. Materials Characterization 2019; 154:161–168.
4. Sroka M., Zieliński A., Hernas A., Kania Z., Rozmus R., Tański T., Śliwa A. The effect of long-term impact of elevated temperature on changes in the microstructure of Inconel 740H alloy. Metalurgija 2017: 56(3-4): 333-336.
5. Zieliński A., Sroka M., Dudziak T. Microstructure and Mechanical Properties of Inconel 740H after Long-Term Service. Materials 2018; 11: 2130.
6. Zalecki W., Rońda J., Gnot A. High temperature properties of Inconel 625 and Inconel 718 alloys. Works of IMŻ 2013; 3: 35-41.
7. Sroka M., Zieliński A., Jonšta Z., Jonšta P. The influence of long-term temperature on the properties and structure of the Inconel 617 welded joint. In: Conference Proceedings of 27th International Conference on Metallurgy and Materials, 2018, 861-866.
8. Ramkumar K.D., Patel S.D., Praveen S.S., Choudhury D.J., Prabaharan P., Arivazhagan N. M.A. Xavior, Influence of filler metals and welding techniques on the structure-property relationships of Inconel 718 and AISI 316L dissimilar weldments. Materials & Design 2014; 62: 175–188.
9. Ramkumar N.T., Selvakumar M., Narayanasamy P., Begam A.A., Mathavan P. Studies on the structural property, mechanical relationships and corrosion behaviour of Inconel 718 and SS 316L dissimilar joints by TIG welding without using activated flux. Journal of Manufacturing Processes 2017; 30: 290–298.
10. Pakieła Z. Microstructure and mechanical properties of Inconel 625 superalloy. Materials Engineering in Plastic Treatment 2010; 3: 143-154.
11. Aircraft material norm SAE AMS 5599F, Nickel alloy, corrosion and heat resistant, sheet, strip and plate 62Ni-21,5Cr-9,0Mo-9,0(Cb+Ta), aneelead UNS NO6625.
12. Rodriguez R., Hayes R.W., Berbon P.B., Lavernia E.J. Tensile and creep behavior of cryomilled Inco 625. Acta Materialia 2003; 51: 911–929.
13. Shankar V., Bhanu Sankara Rao K., Mannan S.L. Microstructure and mechanical properties of Inconel 625 superalloy. Journal of Nuclear Materials 2001; 288: 222-232.
14. Golański G., Słania J., Sroka M., Wieczorek P., Urzynicok M., Krawczyk R. Microstructure and mechanical properties of modern 11% Cr heat-resistant steel weld joints. Materials 2021; 14(12): 3430.
15. Munteanu A. The electron beam welding of dissimilar materials – case study. In: Proc. of IOP Conference Series: Materials Science and Engineering, 2016, 161, 012058.
16. Kah P., Shrestha M., Martikainen J. Trends in Joining Dissimilar Metals by Welding, Applied Mechanics and Materials 2014; 440: 269-276.
17. Cortes R., Barragan E.R., Lopez V.H., Ambriz R.R., Jaramillo D. Mechanical properties of Inconel 718 welds performed by gas tungsten arc welding. The International Journal of Advanced Manufacturing Technology 2018; 94: 3949–3961.
18. Lin H.L., Wu T.M., Cheng C.M. Effects of flux precoating and process parameter on welding performance of inconel 718 alloy TIG welds. Journal of Materials Engineering and Performance 2014; 23: 125–132.
19. Iturbe A., Hormaetxe E., Garay A., Arrazola P.J. Surface integrity analysis when machining Inconel 718 with conventional and cryogenic cooling. Procedia CIRP 2016; 45: 67–70.
20. Węglowski M., Blacha S.A. Phillips: Electron beam welding – techniques and trends – review. Vacuum 2016; 130 72-92.
21. Węglowski M., Dworak J., Błacha S. Electron beam welding and its characteristics. Institute of Welding Bulletin 2014; 58(3): 5-14.
22. Kaur A., Ribton C., Balachandaran W. Electron beam characterisation methods and devices for welding equipment. Journal of Materials Processing Technology 2015; 221: 225–232.
23. Ramkumar K.D., Sidharth Dev, Phani Prabhakar K.V., Rajendran R., Giri Mugundan K., Narayanan S. Microstructure and properties of Inconel 718 and AISI 416 laser welded joints, Journal of Materials Processing Technology 2019; 266: 52–62.
24. Alizadeh-Sh M., Marashi S.P.H., Pouranvari M. Resistance spot welding of AISI 430 ferritic stainless steel: Phase transformations and mechanical properties. Materials & Design 2014; 56: 258-263.
25. Sroka M., Jonda E., Węglowski M., Błacha S. The corrosion studies of electron beam welded nickel alloy. In: Proc. of International Conference on Materials Science and Manufacturing Engineering MATEC Web of Conferences 2019, 253, 03005.
26. Ramkumar K.D., Abraham W.S., Viyash V., Arivazhagan N., Rabel A.M. Investigations on the microstructure, tensile strength and high temperature corrosion. Journal of Manufacturing Processes 2017; 25: 306 –322.
27. Mithilesh P., Varun D., Ajay Reddy Gopi Reddy, Devendranath Ramkumar K., Arivazhagan N., Narayanan S. Investigations on Dissimilar Weldments of Inconel 625 and AISI 304. Procedia Engineering 2014; 75: 66-70.
28. Wiedniga C., Lochbichler C., Enzinger N., Beal C., Sommitscha C. Dissimilar Electron Beam Welding of Nickel base Alloy 625 and 9% Cr Steel. Procedia

Engineering 2014; 86: 184-194.

29. PN-EN ISO 17475 : 2010, Polish standard: Corrosion of metals and alloys – Electrochemical test methods. Guidelines for the performance of potentiostatic and potentiodynamic polarization measurements.
30. Emadi M., Mostaan H., Rafiei M. Experimental Investigation on the dissimilar laser weld joints between Inconel 625 superalloy and AISI 430 ferritic stainless steel. Journal of Advanced Materials and Processing 2020; 8(1): 3-19.
31. Kou S. Welding metallurgy. Jon Wily & Sons Inc, 2003.
32. Arivazhagan N., Singh S., Prakash S., Reddy G.M. Investigation on AISI 304 austenitic stainless steel to AISI 4140 low alloy steel dissimilar joints by gas tungsten arc, electron beam and friction Welding, Materials & Design 2011; 32: 3036-3050.
33. Ramkumar K.D., Mulimani S.S., Ankit K., Kothari A., Ganguly S. Effect of grain boundary precipitation on the mechanical integrity of EBW joints of Inconel 625. Materials Science & Engineering A 2021; 808: 140926.
34. Huang C.A., Wang T.H., Lee C.H., Han W.C. A study of the heat-affected zone (HAZ) of an Inconel 718 sheet welded with electron-beam welding (EBW). Materials Science and Engineering A 2005; 398; 275–281.
35. Moteshakker A., Danaee I. Microstructure and Corrosion Resistance of Dissimilar Weld-Joints between Duplex Stainless Steel 2205 and Austenitic Stainless Steel 316L. Journal of Materials Science & Technology 2016; 32(3): 282-290.